Isolated Impact of Ruffling on the Vibrational Spectrum of Ni Porphyrins. Diagnosing Out-of-Plane Distortions

Hui-Hsu (Gavin) Tsai[†] and M. Cather Simpson*

Center for Chemical Dynamics, Department of Chemistry, Case Western Reserve University, Cleveland, Ohio 44106

Received: September 26, 2003; In Final Form: November 23, 2003

The intrinsic effect of the B_{1u} ruffling (ruf) distortion on the heme vibrational frequencies was evaluated using density functional theory (B3LYP/6-31G(d,p)). Ni(II) porphine (NiP) was constrained for a wide range ruffling angles (τ_{ruf} = the cross macrocycle $C_\alpha-N\text{---}N-C_\alpha$ angle), but otherwise freely geometry optimized, and vibrational frequencies were calculated at each point. This approach allowed the impact of the out-of-plane distortion to be isolated from complicating factors arising from peripheral substituents, the environment, and the metal−macrocycle interaction. The potential energy surface revealed a minimum energy structure at $\tau_{ruf} = 22.8°$ and a small barrier at the planar conformation of 0.162 kcal mol^{-1}. A clear pattern of vibrational shifts driven by the ruffling distortion was observed. Seven degenerate and 17 nondegenerate modes shift by >10 cm^{-1} upon ruffling by 45°. In general, shifts to lower frequencies were seen for higher frequency modes and vice versa. The in-plane asymmetric $C_\alpha-C_m$ stretches $\nu_{10}(B_{1g})$, $\nu_{19}(A_{2g})$, and $\nu_{37}(E_u)$ showed the largest downshifts with ruffling, followed closely by their symmetric counterparts $\nu_3(A_{1g})$, $\nu_{28}(B_{2g})$, and $\nu_{39}(E_u)$ and the $C_\beta-C_\beta$ stretches $\nu_2(A_{1g})$, $\nu_{11}(B_{1g})$, and $\nu_{38}(E_u)$. The Ni−N stretches ν_8 and ν_{18} upshifted significantly, as did some of the in- and out-of-plane pyrrole motions, most notably $\nu_{53}(E_u)$ and $\gamma_{22}(E_g)$. The vibrational shifts were fit excellently by a $\cos(\tau_{ruf})$ function, indicating that the major influence of OOP ruffling upon the vibrational spectrum, and probably porphyrin chemistry and photochemistry as well, is reduced π-overlap.

I. Introduction

Metalloporphyrins perform many useful functions in both biology and technology. For some time now, nonplanar distortions of the porphyrin macrocycle have been implicated in controlling or influencing such functions (for reviews, see refs 1−3). Redox potentials,[4−10] axial ligand binding affinities and dynamics,[11,12] catalytic enantioselectivity,[13,14] and basicity and both the biological and nonbiological insertion of metal ions[15−23] are among the many functional properties shown to be sensitive to deformations of the macrocycle out of plane. In addition, conserved nonplanar features of porphyrins in biological active sites strongly suggest that there are functional biochemical consequences of macrocycle nonplanarity.[1,24−27] This type of regulation of reactivity thus could have consequences ranging from improved fuel cell performance to controlled enzyme efficiency.

It is important, then, to thoroughly understand the fundamental impact of out-of-plane (OOP) distortions upon porphyrin electronic and nuclear structures. The macrocycle is conjugated and therefore nominally expected to be planar. Nonplanar geometries arise as a consequence of the electronic and steric effects of peripheral substituents and the nature of the metal ion−macrocycle interaction. Despite the size and flexibility of the macrocycle, only a limited number of OOP deformations are frequently seen. Scheidt and Lee initiated a useful descriptive nomenclature of ruffling (ruf), saddling (sad), and so forth to identify these common OOP distortions.[28,29] An important refinement was made by Shelnutt and co-workers, who developed a characterization of nonplanarity in terms of linear combinations of the normal modes of the planar species (normal-coordinate structural decomposition; NSD).[25,27,30] Complexly deformed macrocycles can be described as mixtures of the primary distortions ruf, sad, domed (dom), waved (wav), etc.

Several experimental tools are available to build an understanding of the mechanism(s) by which nonplanar distortions affect the porphyrin's chemical and photochemical behavior. Among the more potentially valuable of these are UV−visible and vibrational spectroscopies. Much effort has gone into elucidating the effects of OOP distortions upon the UV−visible absorption spectrum in particular (for reviews, see ref 2 and 3). Numerous experimental studies have led to wide acceptance that OOP distortions induce a red-shift in the major UV−visible absorption bands.[1−7,27,31−35] Correlations of these shifts with the degree and type of distortion have been made; however, recent studies have generated some controversy concerning the reliability of these correlations.[36−41] In fact, although many studies have addressed the impact of OOP distortions upon the UV−visible spectrum, this observable has too little structural detail and is influenced by too many other factors to allow definitive statements concerning OOP distortions to be based upon it alone.

In contrast, the porphyrin vibrational spectrum is rich in information, giving it the potential to provide a more robust analysis, particularly when complemented by other techniques such as UV−visible spectroscopy. Several experimental studies have examined the impact of various OOP distortions upon the macrocycle modes, and correlations with several high-frequency modes promise much for this approach.[31,33−35,42−52] However, a complete understanding of the structure-spectrum relationship

* Corresponding author. E-mail: mcs9@po.cwru.edu.
[†] Current address: Basic Research Program, SAIC−Frederick, Inc., Laboratory of Experimental and Computational Biology, National Cancer Institute−Frederick Cancer Research and Development Center, Building 469, Room 151, Frederick, MD 21702.

10.1021/jp036880w CCC: $27.50
Published on Web 01/20/2004

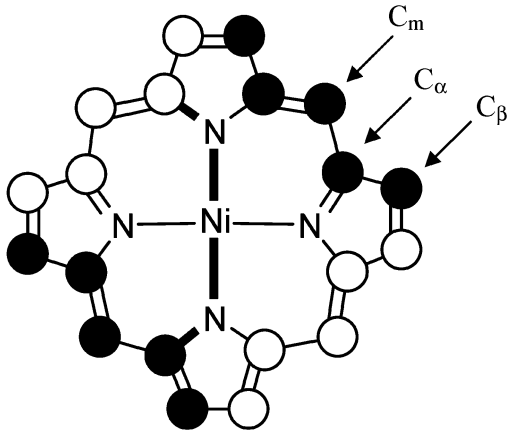

Figure 1. Ni(II) porphine. Atoms that move above and below the plane in the B_{1u} ruffling (ruf) distortion are indicated by open and closed circles. One of the eight equivalent ruffling angles (τ_{ruf}) is shown in bold.

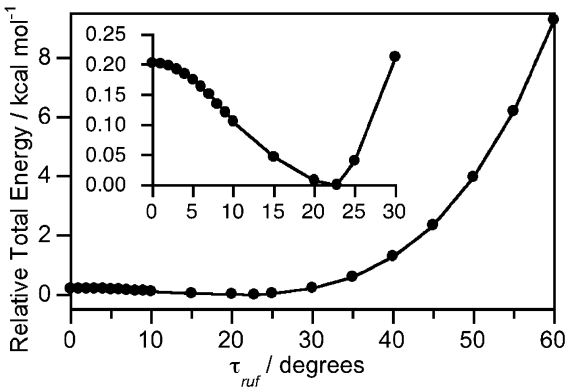

Figure 2. Potential energy along the B_{1u} ruffling coordinate of Ni(II) porphine. Each potential energy point represents a geometry optimization at the B3LYP/6-31G(d,p) level. The τ_{ruf} angles were constrained, but all other variables were allowed to freely optimize. Values are relative to the 22.8° minimum energy point and the zero-point vibrational energy calculated at each point has been included.

is lacking, in part because few high-level computational studies have been attempted. Advances in computational methods and computer speed and memory have led to increasing use of high-level quantum chemistry in the study of porphyrin geometries and energies (for recent reviews, see refs 53 and 54). It is only recently, though, that the computational machinery has progressed to the point of allowing routine calculations of the vibrational spectra of such large, complex systems.

Our objective was to thoroughly and systematically characterize the effect of OOP deformation upon the porphyrin vibrational structure using density functional theory (DFT). One of the major problems that plagues both experimental and theoretical studies of porphyrin nonplanarity is that the procedure for inducing the OOP distortion usually has complicating side effects. Peripheral substituents and the central metal ion impact the rest of the geometry, the electronic structure, vibrational behavior, and other chemical and photophysical properties. The entanglement of these effects makes data interpretation tricky. It becomes quite difficult to attribute observed phenomena to the OOP distortion under study, as the recent controversy about the red-shift in the UV−visible spectrum attests.

To isolate the OOP distortion from these complicating factors, we analyzed constrained porphine geometries (i.e., −H = all substituents). Geometry optimizations and frequency calculations were executed using the B3LYP functional and a relatively large basis set (6-31G(d,p)) on Ni(II) porphine (NiP; Figure 1) at fixed ruffling angles (τ_{ruf} = cross-macrocycle C_α−N---N−C_α angle). NiP was chosen for several reasons. Ni porphyrins are susceptible to OOP deformations, particularly ruf, because the unstrained Ni−N bond length is shorter than can be accommodated by a planar macrocycle.[55] Also, as the "industry standard", Ni porphyrins have been extensively studied and experimental results to which to compare our computational ones are available. Our findings very clearly show the pattern of vibrational shifts that accompanies ruffling. We associate these shifts with physical changes and thereby obtain valuable insight into the structure−spectrum relationship. Comparisons with experimental findings strongly support the diagnostic value of this approach. The results also provide new information that will aid in studies of novel porphyrins. This represents the first such systematic study of the porphyrin vibrational spectrum with high level theoretical methods, to our knowledge.

II. Computational Methods

All geometry optimizations and harmonic frequency calculations were performed on a PC platform using the Gaussian 98 suite of programs.[56] The B3LYP density functional (Becke's three-parameter exchange functional[57] and the Lee−Yang−Parr gradient-corrected correlation functional[58]) was employed. All calculations used the moderate-sized 6-31G(d,p) basis set[59] for all atoms, including Ni. The appropriateness of these functional and basis set choices has been previously discussed.[60] The potential energy surface of NiP along the B_{1u} ruffling coordinate was calculated by constraining the eight equivalent τ_{ruf} angles (Figure 1) while the remaining molecular coordinates were allowed to fully optimize under D_{2d} symmetry. The energies reported include the zero-point vibrational energies. For a subset of structures near 0° ruffling angle, computations with both "tight" (max. force = 0.000015 au; rms force = 0.000010 au; max. displacement = 0.000060 au; rms displacement = 0.000040 au) and "verytight" convergence limits (max. force = 0.000002 au; rms force = 0.000001 au; max. displacement = 0.000006 au; rms displacement = 0.000004 au) were performed. No significant energy or geometry differences were found. All other computations utilized the "tight" convergence limit. The default convergence limits (max. force = 0.000450 au; rms force = 0.000300 au; max. displacement = 0.001800 au; rms displacement = 0.001200 au) were not used. Harmonic vibrational frequencies were calculated to establish correlations with ruffling angle. Fits of vibrational frequencies to ruffling angle were performed using Microcal Origin 6.0 software.

Normal-coordinate structural decomposition (NSD) was performed on the τ_{ruf} = 22.8° (minimum energy) and τ_{ruf} = 45° (constrained) geometries using Version 2.0 of the NSD program (http://jasheln.und.edu/jasheln/default.asp accessed November 22, 2003). The extended basis set was used.

III. Results

Potential Energy along B_{1u} Ruffling Coordinate. The minimum energy geometry at the B3LYP/6-31G(d,p) level was found to have a τ_{ruf} of 22.8°. Figure 2 shows a potential energy surface that is very flat from 0° to ∼30° but increases sharply for larger τ_{ruf}. There is one minimum and a barrier at 0°. The energy difference between the 22.8° minimum and the planar barrier is quite small (0.162 kcal mol^{-1}). There is a single imaginary frequency along the ruffling coordinate (−23 cm^{-1})

for the planar maximum structure; all frequencies are real for the minimum energy conformer.

A computational artifact illustrating the care with which these calculations must be interpreted was encountered when examining the planar (D_{4h}) structure. Constraining the symmetry to D_{4h} resulted in a very small, narrow, planar minimum; the barrier (0.04 kcal mol^{-1}) between the planar and ruffled minima was at 1°. More stringent convergence tolerances ("verytight") yielded no significant changes (less than ±0.000001 Ha = 0.0006 kcal mol^{-1}). Starting with a nonminimum, planar structure and constraining the τ_{ruf} angles to 0° under D_{4h} symmetry led to a nonsensical total energy, different from all others by ~170 kcal mol^{-1}. The most reliable value was obtained using the same procedure as for all of the other constrained geometries: the starting τ_{ruf} was set near, but not at, the constraint value and D_{4h} symmetry was not used. A barrier at τ_{ruf} = 0° resulted from this approach, and it is this finding that appears in Figure 2. All three of the initial conditions above yielded a single negative frequency associated with the lowest frequency ruffling motion, strongly supporting the presence of a barrier here.

NSD treatment of the τ_{ruf} = 22.8 minimum energy and τ_{ruf} = 45° constrained geometries using the extended (complete) macrocycle basis was performed. The out-of-plane decomposition yielded

$$B_{1u}{}^{22.8}(\text{total}) = (1.0461)\,1B_{1u} + (-0.0070)\,2B_{1u} + (0.0093)\,3B_{1u}$$

and

$$B_{1u}{}^{45}(\text{total}) = (2.0204)\,1B_{1u} + (-0.0131)\,2B_{1u} + (0.0041)\,3B_{1u}$$

All other out-of-plane components were zero. These results indicate that the distortion induced by our constraints is almost entirely the $1B_u$ mode, generally referred to as ruffling. Compare to the decompositions of Ni−tetramethylporphyrin (NiT(Me)P; τ_{ruf} = 38°) and Ni−tetra-*tert*-butylporphyrin (NiT(tBu)P; τ_{ruf} = 56°):

$$B_{1u}{}^{NiT(Me)P}(\text{total}) = (1.8578)\,1B_{1u} + (0.1397)\,2B_{1u} + (0.0656)\,3B_{1u}$$

and

$$B_{1u}{}^{NiT(tBu)P}(\text{total}) = (2.7290)\,1B_{1u} + (0.3229)\,2B_{1u} + (0.1012)\,3B_{1u}$$

respectively, reported by Haddad et al.[40] The higher frequency components are an order of magnitude larger or greater than in our constrained NiPs. In fact, the small components of $2B_{1u}$ and $3B_{1u}$ in the constrained NiP results are likely to be due to coordinate rotation deriving from the differences between the normal coordinate and density functional methods of generating normal mode vectors rather than to any structurally significant deviation from "pure" ruffling. The normal coordinate analysis is likely to be in at least slight error, as it is notoriously underdetermined. Previous comparisons of normal coordinate analysis, scaled quantum mechanics and density functional treatment of porphyrin vibrations support this assessment.[60] In addition, only a single imaginary frequency is observed in all of our calculations, and it is for $1B_{1u}$.

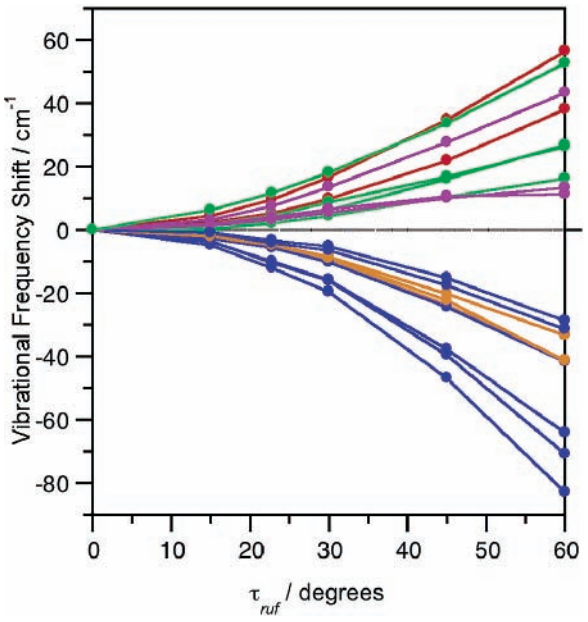

Figure 3. Dependence of selected NiP vibrational frequencies upon the B_{1u} ruffling angle. Vibrational frequencies were calculated at the B3LYP/6-31G(d,p) level upon structures optimized at that same level. The frequencies are reported in Tables 1 and 2. The blue points/lines are $C_\alpha-C_m$ stretches (from bottom to top: ν_{10}, ν_{19}, ν_{37}, ν_3, ν_{39}, and ν_{28}); tan points/lines are $C_\beta-C_\beta$ stretches (from bottom to top: ν_2, ν_{38}, and ν_{11}); the purple points/lines are in-plane pyrrole translations and rotations (from bottom to top: ν_{35}, ν_{33}, and ν_{53}); the green points/lines are out-of-plane pyrrole motions (from bottom to top: γ_{12}, γ_{18}, γ_3, and γ_{22}); and the red points/lines are Ni−N stretches (from bottom to top: ν_{18} and ν_8).

Intrinsic Effects of Ruffling on the Vibrational Spectrum. When treated as a D_{4h} symmetry molecule, NiP's 105 vibrational modes consist of 71 in-plane ($\Gamma_{in-plane}$ = 9 A_{1g} + 9 B_{1g} + 8 A_{2g} + 9 B_{2g} + 18 E_u) and 34 out-of-plane ($\Gamma_{out-of-plane}$ = 5 B_{1u} + 3 A_{1u} + 4 B_{2u} + 6 A_{2u} + 8 E_g) degrees of freedom. Of these, 74 have been experimentally determined (34 nondegenerate and 20 × 2 = 40 doubly degenerate).[61] A_{1g}, B_{1g}, A_{2g}, and B_{2g} modes are enhanced in Raman spectra in resonance with the major $\pi-\pi^*$ absorption bands (B- and Q-bands). Though the E_g modes are also Raman active, they are not enhanced by the B- and Q-band transitions. However, NiP is slightly distorted along the ruffling coordinate in the crystal, and probably in solution as well. This lowering of molecular symmetry to D_{2d} alters the selection rules. The E_g modes become slightly IR active, and the five highest frequency ones have been recently assigned.[61] The E_u and A_{2u} modes are also IR active.

Porphyrin normal modes can be described in dominant local coordinate components, as discussed thoroughly in the literature (for a review, see ref 62). Both local and normal designations are used here. Ruffling lowers the molecular symmetry from square-planar D_{4h} to D_{2d}. The D_{2d} vibrational mode symmetries are correlated with D_{4h} as $A_1 \rightarrow A_{1g}$ and B_{1u}; $B_1 \rightarrow B_{1g}$ and A_{1u}; $A_2 \rightarrow A_{2g}$ and B_{2u}; $B_2 \rightarrow B_{2g}$ and A_{2u}; and $E \rightarrow E_g$ and E_u. For convenience and clarity, D_{4h} notation is used in this study. Mode numbering is consistent with the designations given by Kitagawa and co-workers for Ni(II) octaethylporphyrin.[63,64]

Many of the macrocycle vibrational modes exhibit clear τ_{ruf} dependence (Figure 3, Tables 1 and 2). Both upshifting and downshifting can be observed as the degree of ruffling increases, with several modes moving by greater than 10 cm^{-1} upon ruffling by 45°.

The most strongly downshifted modes are the in-plane $(C_\alpha-C_m)_{asym}$ stretches $\nu_{10}(B_{1g})$, $\nu_{19}(A_{2g})$, and $\nu_{37}(E_u)$, which move

TABLE 1: Dependence of Selected NiP Planar Vibrational Frequencies upon the B_{1u} Ruffling Angle (τ_{ruf})

ruffling angle (τ_{ruf})	ν_i	vibrational frequency (cm^{-1}) exp[a]	B3LYP/6-31G(d,p) 0.0	10.0	20.0	22.8	30.0	45.0	60.0
A_{1g}/A_1									
$\nu(C_\beta C_\beta)$	2	1574	1632	1631	1628	1627	1622	1608	1591
$\nu(C_\alpha C_m)_{sym}$	3	1459	1520	1518	1515	1514	1510	1495	1478
ν(Pyr half-ring)$_{sym}$	4	1376	1416	1417	1417	1417	1417	1416	1414
ν(Pyr breathing)	6	995	1022	1023	1026	1026	1030	1039	1050
δ(Pyr def)$_{sym}$	7	732	745	745	745	745	745	746	745
ν(NiN)	8	369	372	375	380	382	389	407	429
B_{1g}/B_1									
$\nu(C_\alpha C_m)_{asym}$	10	1650	1713	1711	1705	1701	1694	1667	1630
$\nu(C_\beta C_\beta)$	11	1505	1568	1568	1565	1564	1560	1548	1535
ν(Pyr half-ring)$_{sym}$	12	1383	1428	1427	1426	1427	1426	1424	1424
ν(Pyr breathing)	15	1003	1026	1028	1029	1029	1032	1037	1045
δ(Pyr def)$_{sym}$	16	732	748	747	747	747	746	746	746
ν(NiN)	18	237	236	237	240	241	246	258	274
A_{2g}/A_2									
$\nu(C_\alpha C_m)_{asym}$	19	1611	1669	1668	1662	1659	1653	1630	1599
ν(Pyr quarter-ring)	20	1354	1399	1399	1398	1396	1396	1391	1385
ν(Pyr half-ring)$_{asym}$	22	1005	1032	1032	1032	1032	1033	1035	1036
δ(Pyr def)$_{asym}$	24	806	819	819	818	817	816	812	807
δ(Pyr rot.)	25	429	441	440	440	439	439	439	438
B_{2g}/B_2									
$\nu(C_\alpha C_m)_{sym}$	28	1505	1554	1554	1552	1551	1549	1539	1525
ν(Pyr quarter-ring)	29	1368	1401	1400	1400	1400	1399	1396	1393
ν(Pyr half-ring)$_{asym}$	30	1062	1084	1084	1086	1087	1088	1092	1097
δ(Pyr def)$_{asym}$	32	819	832	833	833	834	834	836	836
δ(Pyr rot.)	33	435	439	440	441	442	444	449	452
δ(Pyr trans)	35	- - -	241	242	244	245	247	251	252
E_u/E									
$\nu(C_\alpha C_m)_{asym}$	37	1592	1651	1650	1644	1641	1635	1613	1587
$\nu(C_\beta C_\beta)$	38	1547	1606	1605	1602	1601	1597	1583	1564
$\nu(C_\alpha C_m)_{sym}$	39	1462	1518	1518	1515	1514	1511	1500	1486
ν(Pyr quarter-ring)	40	1385	1428	1427	1427	1428	1427	1427	1428
ν(Pyr half-ring)$_{sym}$	41	1319	1362	1361	1360	1359	1357	1349	1338
ν(Pyr half-ring)$_{asym}$	44	1037	1061	1061	1061	1062	1063	1066	1068
ν(Pyr breathing)	47	995	1019	1020	1023	1023	1026	1034	1044
	50	420	422	420	420	420	422	430	439
δ(Pyr rot.)	49	366	377	377	378	378	380	382	384
δ(Pyr trans)	53	289	300	301	306	307	313	327	343

[a] From ref 61.

to lower frequency by 46, 39, and 38 cm^{-1}, respectively, for a 45° ruffled porphyrin. Their symmetric counterparts, $\nu_3(A_{1g})$, $\nu_{28}(B_{2g})$, and $\nu_{39}(E_u)$, also downshift significantly, by 25, 15, and 18 cm^{-1}, respectively. The $C_\beta-C_\beta$ stretches $\nu_2(A_{1g})$, $\nu_{11}(B_{1g})$, and $\nu_{38}(E_u)$ experience large downshifts with increasing τ_{ruf} as well. Ruffling from 0° to 45° decreases the resonant frequencies of these modes by 24, 20, and 23 cm^{-1} respectively. The only OOP motion that downshifts significantly is A_{2u} doming (γ_9). This mode shifts by 14 cm^{-1} for the 45° ruffled conformer relative to the planar.

Several modes shift to much higher frequencies. The Ni−N stretches $\nu_8(A_{1g})$ and $\nu_{18}(B_{1g})$ shift strongly, by 35 and 22 cm^{-1}, respectively ($\Delta\tau_{ruf} = 0 \rightarrow 45°$). The other Ni−N stretch ($\nu_{50}(E_u)$) also upshifts, though by much less for the same degree of distortion (8 cm^{-1}). Other modes that upshift significantly include the OOP pyrrole motions of saddling ($\gamma_{18}(B_{2u})$), propeller twisting ($\gamma_3(A_{1u})$), and swiveling ($\gamma_{12}(B_{1u})$ and $\gamma_{22}(E_g)$), with changes of 16, 17, 10, and 34 cm^{-1}, respectively ($\Delta\tau_{ruf} = 0 \rightarrow 45°$). Increased frequencies of 10, 10, and 27 cm^{-1} were found for in-plane pyrrole rotation ($\delta_{33}(B_{2g})$) and pyrrole translations ($\delta_{35}(B_{2g})$ and $\delta_{53}(E_u)$) over the same range of ruffling angles. Finally, the pyrrole breathing modes $\nu_6(A_{1g})$, $\nu_{15}(B_{1g})$ and $\nu_{47}(E_g)$ also move to higher frequency with increased ruffling, by 17, 11 and 15 cm^{-1}, respectively, from $\tau_{ruf} = 0°$ to 45°.

TABLE 2: Dependence of Selected NiP Nonplanar Vibrational Frequencies upon the B_{1u} Ruffling Angle (τ_{ruf})

ruffling angle (τ_{ruf})	γ_i	vibrational frequency (cm^{-1}) exp[a]	B3LYP/6-31G(d,p) 0.0	10.0	20.0	22.8	30.0	45.0	60.0
B_{1u}/A_1									
−yr swivel	12		697	697	698	699	701	707	713
$\gamma(C_m C_\alpha C_m C_\alpha)$	13		467	468	469	469	471	476	480
A_{1u}/B_1									
(Pyr fold)$_{asym}$	1		685	685	684	684	684	681	677
propeller	3		269	271	273	274	278	286	296
B_{2u}/A_2									
(Pyr fold)$_{sym}$	15		653	652	653	654	655	657	661
Pyr tilt	16		241	239	239	239	238	235	230
saddle	18		34	32	35	37	40	50	61
A_{2u}/B_2									
$\gamma(H_m C_\alpha C_m C_\alpha)$	4	854	873	873	870	870	870	871	865
(Pyr fold)$_{sym}$	5	768	778	777	776	775	775	774	773
$\gamma(C_m C_\alpha C_m C_\alpha)$	6	698	704	705	706	707	710	715	723
Pyr tilt	7	357	349	348	349	349	350	355	361
$(H_\beta C_\beta - C_\beta H_\beta)_{sym}$	8	282	263	263	264	264	266	271	281
dome	9	108	108	107	105	104	101	94	83
E_g/E									
$\gamma(H_m C_\alpha C_m C_\alpha)$	19	844	863	862	861	860	861	862	858
(Pyr fold)$_{asym}$	20	776	789	788	787	786	785	784	781
(Pyr fold)$_{sym}$	21	896	916	916	915	915	915	915	914
Pyr swivel	22	418	425	428	434	437	443	459	477
Pyr tilt	23	656	671	671	671	671	671	671	670

[a] From ref 61.

IV. Discussion

Relatively rapid advances in computing power and quantum chemistry software have made high level calculations on porphyrins feasible on a relatively routine basis. The remarkable progress in this area has been recently reviewed by Ghosh.[53,54] Several quantum mechanical studies have focused upon the effects of out-of-plane distortions upon porphyrin spectrum and function. Most have used peripheral substituents, with or without imposed constraints, to induce the porphyrin to adopt a nonplanar geometry. Though these studies have provided insight into the structure−spectrum relationship, the electronic and steric effects of the substituents complicate the analyses, making it difficult to clearly dissect out the effects of the OOP distortion on the porphyrin spectrum and function. We therefore chose to study the effects of OOP distortions by performing DFT calculations on porphine (−H substituents only) constrained along OOP coordinates, beginning with ruffling. The systematic and isolated effect of ruffling upon the vibrations is discussed here.

As UV−visible spectroscopy appears to have limitations when used by itself to indicate macrocycle nonplanarity, we chose to focus upon the vibrational spectrum. Experimental studies of the effects of ruffling upon vibrational frequencies are relatively abundant, but only limited theoretical exploration has been reported.[52,61,65,66] The goals, therefore, were (1) to establish correlations between τ_{ruf} and several OOP-sensitive vibrational frequencies such that (2) a pattern of shifts could be used to characterize the type and magnitude of OOP distortion experimentally, and (3) to provide physical insight into the response of the vibrational spectrum to macrocycle ruffling.

Generally, it is not wise to calculate vibrational frequencies at geometries that are not at the minimum energy point. This study illustrates a special case where such an approach is legitimate. The constraint employed generates a distortion along a normal mode. The geometry is optimized along all of the other coordinates. As these other coordinates are orthogonal to the

TABLE 3: Dependence of Selected Geometry Parameters upon the B_{1u} Ruffling Angle (τ_{ruf})

τ_{ruf}/deg	Ni−N/Å	$C_\alpha-C_m$/Å	$C_\alpha-C_\beta-C_\beta-C_\alpha$/deg	$C_\beta-C_\alpha-C_m-C_\alpha$/deg	$N-C_\alpha-C_m-C_\alpha$/deg
0.0	1.9569	1.3793	0.0	180.0	0.0
22.8	1.9425	1.3815	1.9	169.1	5.4
45.0	1.9036	1.3884	3.4	159.0	9.4
60.0	1.8691	1.3961	4.0	152.5	10.9

constrained one, optimization finds their minima. Their computed vibrational frequencies are thus valid. Only one negative frequency is found, and it is associated with the lowest frequency B_{1u} ruffling mode. Analysis of this particular frequency is problematic at best, and is not attempted here.

Our systematic examination of the NiP potential energy along the ruffling coordinate reveals a fairly flat surface with a minimum at 22.8° and a small barrier (0.2 kcal mol^{-1}) at 0°. This result is not unexpected, in light of previous calculations of the NiP minimum energy geometries reported by ourselves and others.[60,61] It is consistent also with calculated potential surfaces for six-coordinate P^V and Si^{IV} porphyrins and porphyrin ions[65] and with recent DFT studies of Ni(II) tetraphenylporphyrin (NiTPP)[52] and Ni(II) octaethylporphyrin.[67] Ni porphyrins are particularly susceptible to the ruffling distortion, as it allows the Ni−N bond to contract to a more energetically favored value.[55] This shortening occurs at the expense of conjugation, and presumably it is the nature of this interplay that generates the very flat potential energy surface for NiP along τ_{ruf}.

The position of the balance point and the height of the barrier at 0° = τ_{ruf} differ, depending upon the method and basis set employed. For example, B3LYP/6-31G(d)/VTZ(Ni),[61] B3LYP/6-311G,[61] and BLYP/6-31G(d,p)[60] optimizations of NiP found minimum energy geometries at τ_{ruf} = 12°, 20°, and 29°, respectively. The corresponding barriers at D_{4h} symmetry were calculated to be 0.002, 0.105, and 0.563 kcal mol^{-1}. The levels of theory employed by these studies are comparable and high. Though the results seem at first glance to be widely disparate, they are actually in agreement about the major findings: NiP prefers to be ruffled and a small (<1 kcal mol^{-1}) barrier exists at the planar configuration. Further analysis (i.e., argument concerning the exact ruffling angle and barrier height) is not warranted, given the current level of accuracy of DFT.[68]

Previous, more limited studies anticipated a soft potential for moderate ruffling and a very small planar barrier that we found in our computations. However, we have extended characterization into the functionally important and largely ignored highly deformed region of the PES beyond τ_{ruf} = 30°. We have also provided an unprecedented level of detail in the picture of the energetic consequences of ruffling. Figure 2 shows how rapidly the energetic costs accelerate for τ_{ruf} beyond the minimum energy point. It takes a comparable amount of energy for the porphyrin to un-ruffle by 23° from the minimum as it does for it to ruffle further by only 8°. Still, very large ruffling angles (e.g., τ_{ruf} = 60°) can be achieved with relatively modest energy expenditures (<10 kcal mol^{-1}).

The flat nature of the potential indicates that the geometry of NiP is likely to be quite sensitive to the molecular environment. Indeed, the crystal structure is only very slightly ruffled, with a τ_{ruf} = 1.7°.[49] In solution, the insensitivity of the resonance Raman depolarization ratio to the excitation energy indicates that the macrocycle is nearly planar under those conditions as well.[69] Taken together, the computations and experiments support a picture in which any planar barrier is so small that there is effectively a single, wide, shallow potential.

The flatness of the PES belies the sensitivity of some aspects of porphyrin behavior, including portions of the vibrational spectrum, to the ruffling angle. The vibrational modes shift in a characteristic pattern with ruffling (Figure 3, Tables 1 and 2). The shifts are measurable, though moderate, from τ_{ruf} = 0° to the minimum energy structure at τ_{ruf} = 22.8°, and accelerate thereafter. Seven degenerate and 17 nondegenerate modes shift >10 cm^{-1} upon ruffling by 45°; some modes downshift and some move to higher frequencies. In general, shifts to lower frequencies were seen for higher frequency modes, whereas lower frequency modes tend to upshift.

Physical insight can be acquired by analyzing the vibrational changes in terms of alterations in the geometry and electronic distribution. Ruffling inherently affects the in-plane (bond lengths and bond angles) and out-of-plane (torsion angles) macrocycle degrees of freedom, even in the absence of complications from metal ion, ligation, and peripheral substituent electronic and steric effects. This OOP deformation significantly affects both the metal-macrocycle interaction and the p-orbital overlap that gives rise to the long range conjugation across the molecule. These are the primary physical origins of the ruffling-induced changes in the porphyrin geometry. The impact of ruffling on the macrocycle geometry is more fully elaborated elsewhere;[70] salient features are summarized here in Table 3.

The most noticeable in-plane alteration accompanying ruffling is the shortening of the Ni−N bonds. This phenomenon has been thoroughly discussed in the literature.[3,29,55,71] Briefly, the core of a planar porphyrin macrocycle is too large to accommodate unstrained Ni−N bonds. These bonds would prefer to be on the order of 1.85 Å but are forced to lengthen to 1.95 Å or so in the planar NiP. As the NiP ruffles, the pyrrole rings relax inward, toward the central metal ion, and the Ni−N bond lengths shorten considerably. By τ_{ruf} = 45°, the bond length has shortened from its planar value (1.957 Å) by 2.7% to 1.904 Å. Energetically, this contraction provides part of the driving force for ruffling.

Ruffling can be envisioned as the pyrroles twisting relative to each other while maintaining individual planarity, so that ruffling is accommodated primarily by the $C_\alpha-C_m-C_\alpha$ architecture. In ruffling from 0° to 45°, the pyrrole torsion $C_\alpha-C_\beta-C_\beta-C_\alpha$ changes by only 3.4°. Except for the Ni−N bonds, the $C_\alpha-C_m$ bond lengths change by almost twice as much or more than the other bond lengths. They lengthen 0.66% from 1.3793 Å at τ_{ruf} = 0° to 1.3884 Å at 45° ruffling. Similarly, the most distorted torsion angles (except τ_{ruf}) are the $X-C_\alpha-C_m-C_\alpha$, which change by 21.0° (X = C_β) and 9.4° (X = N) in going from 0° to 45° ruffling.

The primary consequence of ruffling for the macrocycle behavior derives from the weakening of the macrocycle π-system through reduced overlap of the neighboring p_z orbital (p_z = perpendicular to the plane of the flat macrocycle). The overlap integral associated with two p_z orbitals has a cos(τ) dependence, where τ is the twist angle the orbitals make relative to each other. Bond lengths, molecular orbital energies (and therefore UV−visible transitions), and vibrational frequencies can therefore be expected to exhibit cos(τ_{ruf}) dependence:

$$y = A + B\cos(\tau_{ruf}) \qquad (1)$$

The changes in bond lengths we observed in our B3LYP/6-31G(d,p) calculations obey this cos(τ_{ruf}) dependence quite well.

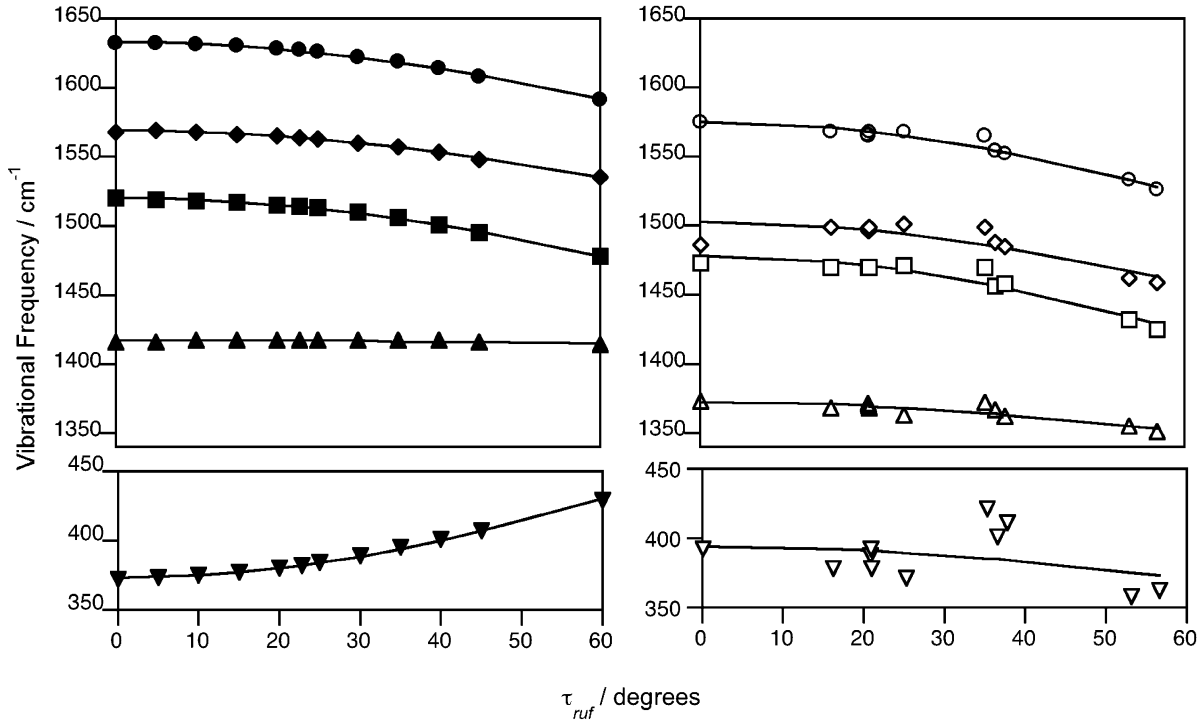

Figure 4. Calculated vibrational frequencies (B3LYP/6-31G(d,p); closed symbols in right panel) and experimental vibrational frequencies[35] (NiTAP series of porphyrins; open symbols in left panel) for ν_2 (circles), ν_{11} (diamonds), ν_3 (squares), ν_4 (triangles) and ν_8 (inverted triangles) were fit using eq 1. The fitting results for the calculated frequencies were ν_2 ($A = 1550.2$, $B = 82.72$, $r^2 = 0.997$), ν_3 ($A = 1436.8$, $B = 83.29$, $r^2 = 0.997$), ν_{11} ($A = 1500.7$, $B = 68.17$, $r^2 = 0.997$), ν_4 ($A = 1413.0$, $B = 4.09$, $r^2 = 0.45$), and ν_8 ($A = 487.4$, $B = -114.18$, $r^2 = 0.998$). The fitting results for the experimental frequencies were ν_2 ($A = 1471.3$, $B = 103.59$, $r^2 = 0.95$), ν_3 ($A = 1368.9$, $B = 109.21$, $r^2 = 0.92$), ν_{11} ($A = 1414.5$, $B = 88.07$, $r^2 = 0.76$), ν_4 ($A = 1329.9$, $B = 42.43$, $r^2 = 0.78$), and ν_8 ($A = 347.8$, $B = 46.11$, $r^2 = 0.12$).

The r^2 correlation is greater than or equal to 0.99 for the Ni−N, C_α−N, C_α−C_m, and C_β−C_β bonds (not shown). The excellent agreement with this simple cosine function strongly supports the hypothesis that the impact of ruffling upon molecular behavior operates through this reduction in π-overlap.

The vibrational frequencies are affected by ruffling in complete accordance with these physical underpinnings (Figure 4). Examination of the downshifted modes illustrates this. The most strongly shifted are the in-plane $(C_\alpha-C_m)_{asym}$ stretches $\nu_{10}(B_{1g})$, $\nu_{19}(A_{2g})$, and $\nu_{37}(E_u)$, which move to lower frequency by 46, 39, and 38 cm^{-1}, respectively, for a $\tau_{ruf} = 45°$ ruffled porphyrin. The symmetric C_α−C_m stretches, $\nu_3(A_{1g})$, $\nu_{28}(B_{2g})$, and $\nu_{39}(E_u)$, shift nearly as much by 25, 15, and 18 cm^{-1}, respectively, for the same ruffling angle. Mentioned above, much of the strain of the ruffling distortion is taken up in C_α−C_m−C_α architecture. The C_α−C_m bond lengthens appreciably and the torsions about the C_α−C_m bonds are altered significantly. The striking dependence of these modes upon τ_{ruf} is the spectral manifestation of these in-plane and out-of-plane rearrangements.

The C_β−C_β stretches $\nu_2(A_{1g})$, $\nu_{11}(B_{1g})$, and $\nu_{38}(E_u)$ experience downshifts (20−25 cm^{-1}) with increasing τ_{ruf}, comparable to those associated with the C_α−C_m stretches. The C_β−C_β bonds lengthen with ruffling, third in sensitivity to τ_{ruf} only to the Ni−N and C_α−C_m bonds. The downshifting of all of these major in-plane stretches reflects the reduced conjugation about the macrocycle that accompanies the OOP distortion.

The only OOP motion that downshifts appreciably is the A_{2u} doming motion. Ruffling from 0° to 45° induces a shift of 14 cm^{-1} in this mode. This shift is interpreted as coming from the reduction in conjugation that accompanies ruffling as well. Reducing the overall π-overlap about the macrocycle induces the nitrogens to become less sp^2-like. From the perspective of each nitrogen atom, the doming motion is an umbrella-type mode. This motion is softer in the less-strongly conjugated system.

The modes that shift to higher frequencies with ruffling tend to be lower frequency distortions. The Ni−N stretches $\nu_8(A_{1g})$ and $\nu_{18}(B_{1g})$ shift strongly, by 35 and 22 cm^{-1}, in going from the planar to the 45° ruffled form, respectively. The other Ni−N stretch ($\nu_{50}(E_u)$) also upshifts, though by only 8 cm^{-1}. This increase in frequency of the Ni−N stretches with ruffling is explained by the large contraction of the Ni−N bond length that accompanies the OOP distortion. Other modes that upshift significantly include the OOP pyrrole motions of saddling ($\gamma_{18}(B_{2u})$), propeller twisting ($\gamma_3(A_{1u})$), and swiveling ($\gamma_{12}(B_{1u})$, $\gamma_{22}(E_g)$). In-plane pyrrole rotation ($\delta_{33}(B_{2g})$) and pyrrole translation ($\delta_{35}(B_{2g})$, $\delta_{53}(E_u)$) also upshift appreciably. These modes involve motions of whole pyrrole rings relative to one another and hence should be affected by distortions of the links between pyrrole rings. It should be noted that these types of modes are not all similarly affected by ruffling; the frequencies of some are not nearly as sensitive.

Several experimental studies,[31,33−35,42−52] and a few computational ones,[52,61,65,66] have explored the effects of ruffling on the vibrational spectrum. Of particular interest to our inquiries are systems in which the electronic and/or steric effects of the peripheral substituents are at least nominally constant as the molecule ruffles. One of the better suited molecules from this standpoint is Ni(II) octaethyl porphyrin (NiOEP). NiOEP exists in three crystal forms; triclinic A and B are planar, whereas the tetragonal C form is fairly ruffled ($\tau_{ruf} = 33°$).[42,72,73] In solution, the planar and ruffled conformers appear to coexist.[43,44,50] Another relevant system is Ni(II) tetraphenylporphyrin (NiTPP). NiTPP crystallizes ruffled ($\tau_{ruf} \sim 30°$)[51,74] but also exists as a

mixture of ruffled and planar conformers in solution.[51,52] Finally, Shelnutt and co-workers studied a Ni porphyrin system in which the electronic effects of the peripheral, ruffling-inducing substituents are similar but steric influences are not.[35] This series of Ni porphyrins with C_m−alkyl substituents (NiTAPs) exploited increasing substituent bulk to progressively ruffle the macrocycle from ∼0° to >55°. The substituents exerted varying degrees of in-plane and out-of-plane stress on the macrocycle. Our results are entirely consistent with these studies, in most cases on a quantitative level.

Perhaps the best test case for the quantitative accuracy of our vibrational predictions is NiOEP. Here, the peripheral ethyl groups are on the C_β positions where they do not sterically interact with the macrocycle as much as do C_m substituents. They are also relatively electronically benign. That is, their electronic influence should be independent of (reasonable) changes in their orientations. Substituent orientations are invoked to explain the presence of both planar and ruffled crystal structures. The flat PES we observe from $\tau_{ruf} = 0°$ to 30° is quite consistent with the presence of both ruffled and planar solid state conformers and with their coexistence in solution. In fact, as mentioned above the calculated energy difference between the planar and ruffled minimum energy structures of NiP is 0.2 kcal mol^{-1}, similar to that measured experimentally for the energy difference between the planar and ruffled NiOEP conformers (∼0.7 kcal mol^{-1}).[50]

Several of the modes predicted to downshift by our calculations have been observed in the NiOEP spectra. The experimental results are in good quantitative agreement with our findings. In resonance Raman spectra of the triclinic and tetragonal crystals, the asymmetric C_α−C_m stretches ν_{10} and ν_{19} are seen to be the most sensitive to ruffling; they downshift by ∼20 cm^{-1} in the tetragonal (ruffled) relative to the triclinic (planar) species.[42−44,50] Other high-frequency modes ν_2 ($\nu(C_\beta C_\beta)$), ν_{11} ($\nu(C_\beta C_\beta)$), ν_3 ($\nu(C_\alpha C_m)_{sym}$), and ν_{28} ($\nu(C_\alpha C_m)_{sym}$) are observed to shift less strongly (7−13 cm^{-1}) with ruffling. The B3LYP/6-31G(d,p) calculations for the $\tau_{ruf} = 0°$ and $\tau_{ruf} = 30°$ conformers show remarkable agreement with experiment. ν_{10} and ν_{19} are predicted to downshift by 19 and 16 cm^{-1}, respectively, in ruffling from planar to τ_{ruf} conformers. The other four modes (ν_2, ν_{11}, ν_3, and ν_{28}) are predicted to shift by 6−10 cm^{-1}. The ν_4 mode involves motions of the pyrrole atoms with little C_m participation. Our calculations predict that this mode should be independent of ruffling angle. Spectra of the NiOEP crystals support this prediction; the ν_4 frequency is the same for the triclinic and tetragonal forms.[42−44,50]

Comparisons in the lower frequency region, where several modes are predicted to upshift significantly with ruffling, are more tricky. The spectrum is congested and many of the NiOEP modes appear to be sensitive to the ethyl orientational isomerization.[44] The Ni−N stretch mode ν_8 is particularly sensitive, showing quite different frequencies for the two triclinic planar species. An upshift of 7 cm^{-1} is observed for the other Ni−N stretch ν_{18}, which compares favorably to the predicted value of 10 cm^{-1}. The pyrrole translation (δ_{35}) shifts from 143 cm^{-1} in planar NiOEP to 152 cm^{-1} in the ruffled form, slightly more than the 6 cm^{-1} upshift predicted by the NiP calculations. In contrast, the pyrrole rotation $\delta_{33}(B_{2u})$ mode, which is expected to upshift by about 5 cm^{-1}, actually downshifts by 10 cm^{-1} in NiOEP. Thus the above similarities in the low-frequency region may be fortuitous, given the difficulties with isolating the effects of ruffling from those of the ethyl substituents in the experimental system.

The Ni−N stretch ν_8 of NiTPP has been examined experimentally in some detail,[51,52] and the results are very consistent with our computational findings. The spectrum is less congested in this system, and the ν_8 mode seems less sensitive to peripheral substituent orientations. NiTPP exists as a mixture of ruffled and planar conformers in solution. Curvefitting of a solution resonance Raman spectrum gave three bands, two of which were assigned to ν_8, 389 cm^{-1} for the planar and 400 cm^{-1} for the ruffled species, on the basis of intensity analysis and DFT results.[52] The ruffling angle is unknown for the solution conformer, though it is probably less than 30°, by analogy to NiOEP. However, the observed upshift provides strong evidence supporting both the quality and utility of our results.

The third set of experimental findings to which we compare our findings is the NiTAP series.[35] The vibrational changes observed for these molecules contain contributions from both ruffling and other distortions induced by the peripheral substituents. The experimental behavior of the ν_{10} and ν_{19} modes are not discussed, but the trends for ν_2, ν_3, and ν_{11}/ν_{28} are similar to those predicted here. Figure 4 shows a detailed comparison.

As mentioned above, one of the primary consequences of ruffling is loss of π-conjugation. Accordingly, we fit our findings, as well as those of Jentzen et al.,[35] to the function (1).[75] Values for *A*, *B*, and the r^2 correlation parameter are presented in the legend to Figure 4. The fit of our results to (1) is excellent across the whole range of ruffling angles studied. With the exception of ν_4, which shows virtually no dependence upon τ_{ruf}, the r^2 correlation values were ≥0.99 for all of the experimentally important, high-frequency modes (upper panels, Figure 4). The experimental results also fit this function (1), though not as well. The dependence of the ν_2, ν_3, and ν_{11}/ν_{28} modes upon ruffling angle is a bit stronger for the experimental system than for the computations. One possible source of this small difference is substituent effects present in the experimental system but absent in the calculations, including electronic influences and other geometric perturbations (other than the ruffling distortion isolated in our study). For example, the small but significant components of higher energy B_{1u} distortions contributing to the overall structures in the NiTAP experimental study may affect the vibrational frequencies. Other possible sources are the presence of the solvent in the experiment and the fact that the experimental τ_{ruf} are actually calculated by molecular mechanics rather than experimentally determined (see below). In fact, despite these significant differences in the conditions of the experiment and the computations, the nearly quantitative correlations between their vibrational results are excellent and bode well for use of the vibrational spectrum as an indicator of the porphyrin OOP distortions.

One glaring discrepancy between the calculation and NiTAP experiments is for ν_8 (lower panels, Figure 4). Here, even the qualitative trends are not in agreement. The computations predict a strong upshift in ν_8, fit to (1) with an r^2 of 0.998. Characterization of ν_8 in the NiTAPs revealed no consistent correlation with τ_{ruf}, however. Fits of the experimental data to (1) gave a slight downshift with ruffling, but the r^2 value of 0.12 indicates the weakness of this conclusion. The assignment of ν_8 in the experiment is difficult due to spectral congestion, and isotope shifts were not used in making the assignments. Our results suggest that ν_8 has been misassigned in some of the experimental spectra. The scatter in the experiments may be due to extreme sensitivity of ν_8 to substituent effects other than ruffling. However, DFT calculations and experimental findings on ν_8 in NiTPP bolster our conclusion that ruffling

should have the dominant impact on ν_8 and the mode should upshift strongly with increasing τ_{ruf}.

Few computational studies of the vibrational response of the porphyrin to ruffling have been reported, probably due to the relatively challenging size of the calculations. Ghosh and co-workers examined the behavior of the ν_2, ν_3, ν_{11}, and ν_{38} modes of some Ge, Si, and P porphines.[65] In this system, the degree of ruffling is controlled by the identity of the central ion and the fifth and sixth ligands coordinated to it. The range of ruffling angles spanned is quite large: $Ge^{IV}F_2-P$ ($\tau_{ruf} = 0°$), $Si^{IV}Cl_2-P$ (12.8°), $Si^{IV}F_2-P$ (24.2°), $[P^{V}Cl_2-P]^+$ (47.8°), and $[P^{V}F_2-P]^+$ (54.7°). The results are quite different from ours; the frequencies of all four modes increased from $\tau_{ruf} = 0°$ to 12.8°, and then decreased nearly linearly thereafter. The reduced conjugation that accompanies the OOP distortion is clearly not the dominant effect in this system. This dissimilarity underscores the difficulties inherent in such studies of ruffling. The agent used to induce the ruffling has other, often more significant, effects upon the system. Unfortunately, these results cannot help the interpretation of the Ni porphine findings.

A couple of much more directly relevant computations have been performed on four-coordinate Ni(II) porphyrins. Spiro, Pulay, Kozlowski, and co-workers used DFT (B3LYP) and scaled quantum mechanics (SQM) to study the vibrational structure of NiP,[61] NiTPP,[52] and NiOEP.[66] For NiP and NiTPP, vibrational frequencies for the planar (D_{4h}) barrier conformers and for the minimum energy structures at $\tau_{ruf} = 11.8°$ and 32.2°, respectively, are reported. For the NiP study, the shifts in vibrational frequencies are calculated but not discussed, except to note that they are small (<6 cm^{-1}). This is not surprising, given the minor extent of ruffling in the structure they studied. The NiTPP results are quite similar to ours, with the largest shifts being seen for modes involving the $C_\alpha-C_m$ bonds. The magnitudes of the shifts they observe are consistent, for the most part, with those reported here. Differences are most likely due to the presence of the phenyl substutients at the C_m positions. The NiOEP studies computed IR spectra for the tetragonal ruffled ($\tau_{ruf} = 8.4°$), triclinic A planar and ruffled ($\tau_{ruf} = 19.8°$) and triclinic B planar and ruffled ($\tau_{ruf} = 19.1°$) species. Their findings were very similar to ours with the exception of the γ_{22} (OOP pyr swiv) mode, which we predict to upshift by 9 cm^{-1} in a 20° ruffled porphyrin (relative to the planar species), but they observe changes by just 1 cm^{-1}. However, as each of these studies examined only two points on the potential surface, none is able to establish a pattern of shifts that can be used to predict the behavior of other systems.

Examining the details of the potential energy surface along the ruffling coordinate requires a significant investment of time and computational effort. However, the payoff for these additional labors is manifold. We have isolated the effects of the OOP ruf deformation from those of peripheral substituents, the central metal ion, ligation effects and the environment. Our study also provides the means to evaluate the functional form of the dependence of the vibrational spectrum upon ruffling. We can thus examine the underlying physical influences giving rise to the observed behavior. The excellent fit of the vibrational frequency changes to the $\cos(\tau_{ruf})$ function (1) provides strong support for the reduction of conjugation being the primary influence ruffling upon the macrocycle. The match with experiment provides further evidence that this mechanism is most likely to be significant functionally. Examinations of real ruffled porphyrins can utilize our findings to evaluate the intrinsic contribution of the OOP distortion ruf itself to the observed chemical and/or photochemical behavior. In addition, we present the first high-level vibrational calculations on highly distorted Ni porphyrins. This significantly extends the range of ruffling angles studied beyond the relatively flat area from 0° to ~30°. This extension is particularly important because it is ruffling angles of greater than 30° that are expected to have the most significant functional consequences.

The approach presented here also holds out great promise for the vibrational spectrum to be used as a diagnostic tool in establishing the type and extent of OOP deformation of porphyrins. In principle, the vibrational spectrum has sufficient fine structure to distinguish among the major OOP porphyrin conformers. Similar calculations along other important OOP degrees of freedom, such as saddling, doming, and waving, are underway in our laboratory. It is anticipated that comparisons of the sets of vibrational shifts will reveal patterns that can be used to identify and characterize novel porphyrins and porphyrins in environments where the structure is unknown (e.g., in solution).

V. Summary

High-level quantum calculations of the vibrational frequencies along the potential energy surface associated with the B_{1u} ruffling (ruf) coordinate are presented and analyzed. The approach utilized allows unambiguous isolation of the effects of the OOP distortion from complicating factors due to peripheral substituents, the central metal ion, ligation effects, and environmental influences. The results are entirely consistent with a physical picture in which the reduced conjugation about the macrocycle accounts for the observed behavior. The major influence of the OOP ruffling deformation upon porphyrin chemical and photochemical functionality is likely to be via this mechanism as well. Comparisons with appropriate experimental findings show remarkable agreement. The approach presented here thus holds out great promise for the vibrational spectrum to be used as a diagnostic tool in establishing the type and extent of OOP deformation of porphyrins.

Acknowledgment. This work was supported by NIH grant GM056816 (M.C.S.). We thank Dr. R. C. Dunbar (Case) and Dr. J. Protasiewicz (Case) for helpful comments.

References and Notes

(1) Shelnutt, J. A.; Song, X.-Z.; Ma, J.-G.; Jia, S.-L.; Jentzen, W.; Medforth, C. J. *Chem. Soc. Rev.* **1998**, *27*, 31.

(2) Ravikanth, M.; Chandrashekar, T. K. *Struct. Bonding* **1995**, *82*, 105.

(3) Senge, M. O. Highly Substituted Porphyrins. In *The Porphyrin Handbook*; Kadish, K. M., Smith, K. M., Guilard, R., Eds.; Academic Press: New York, 2000; Vol. 1, p 239.

(4) Barkigia, K. M.; Chantranupong, L.; Smith, K. M.; Fajer, J. *J. Am. Chem. Soc.* **1988**, *110*, 7566.

(5) Barkigia, K. M.; Renner, M. W.; Furenlid, L. R.; Medforth, C. J.; Smith, K. M.; Fajer, J. *J. Am. Chem. Soc.* **1993**, *115*, 3627.

(6) Kadish, K. M.; D'Souza, F.; Villard, A.; Autret, M.; Van Caemelbacke, E.; Blanco, P.; Antonini, A.; Tagliatesta, P. *Inorg. Chem.* **1994**, *33*, 5169.

(7) Ochsenbein, P.; Ayougou, K.; Mandon, D.; Fischer, G.; Weiss, R.; Austin, R. N.; Jayaraj, K.; Gold, A.; Terner, J.; Fajer, J. *Angew. Chem., Int. Ed. Engl.* **1994**, *33*, 348.

(8) Kadish, K. M.; Van Caemelbacke, E.; D'Souza, F.; Medforth, C. J.; Smith, K. M.; Tabard, A.; Guilard, R. *Inorg. Chem.* **1995**, *34*, 2984.

(9) Kadish, K. M.; Lin, M.; Van Caemelbacke, E.; De Stefano, G.; Medforth, C. J.; Nurco, D. J.; Nelson, N. Y.; Krattinger, B.; Muzzi, C. M.; Jaquinrod, L.; Xu, Y.; Shyr, D. C.; Smith, K. M.; Shelnutt, J. A. *Inorg. Chem.* **2002**, *41*, 6673.

(10) Renner, M. W.; Barkigia, K. M.; Melamed, D.; Gisselbrecht, J.-P.; Nelson, N. Y.; Smith, K. M.; Fajer, J. *Res. Chem. Intermed.* **2002**, *28*, 741.

(11) Alden, R. G.; Ondrias, M. R.; Shelnutt, J. A. *J. Am. Chem. Soc.* **1990**, *112*, 691.

(12) Retsek, J. L.; Drain, C. M.; Kirmaier, C.; Nurco, D. J.; Medforth, C. J.; Smith, K. M.; Sazanovich, I. V.; Chirvony, V. S.; Fajer, J.; Holten, D. *J. Am. Chem. Soc.* **2003**, *125*, 9787 and references therein.

(13) Perollier, C.; Pecaut, J.; Ramasseul, R.; Marchon, J.-C. *Inorg. Chem.* **1999**, *38*, 3758.

(14) Gazeau, S.; Pecaut, J.; Haddad, R. E.; Shelnutt, J. A.; Marchon, J.-C. *Eur. J. Inorg. Chem.* **2002**, 2956.

(15) Hambright, P.; Shah, B.; Shears, B. *Inorg. Chem.* **1971**, *10*, 1828.

(16) Barkigia, K. M.; Berber, M. D.; Fajer, J.; Medforth, C. J.; Renner, M. W.; Smith, K. M. *J. Am. Chem. Soc.* **1990**, *112*, 8851.

(17) Cochran, A. G.; Schultz, P. G. *Science* **1990**, *249*, 781.

(18) Takeda, J.; Ohya, T.; Sato, M. *Inorg. Chem.* **1992**, *31*, 2877.

(19) Blackwood, M. E. J.; Rush, T. S. I.; Medlock, A.; Dailey, H. A.; Spiro, T. G. *J. Am. Chem. Soc.* **1997**, *119*, 12170.

(20) Blackwood, J., Milton E.; Rush, I., Thomas S.; Romesberg, F.; Schultz, P. G.; Spiro, T. G. *Biochemistry* **1998**, *37*, 779.

(21) Franco, R.; Ma, J.-G.; Lu, Y.; Ferreira, G. C.; Shelnutt, J. A. *Biochemistry* **2000**, *39*, 2517.

(22) Finikova, O. S.; Cheprakov, A. V.; Carroll, P. J.; Dalosto, S.; Vinogradov, S. A. *Inorg. Chem.* **2002**, *41*, 6944.

(23) Yin, J.; Andryski, S. E.; Beuscher, A. E. T.; Stevens, R. C.; Schultz, P. G. *Proc. Natl. Acad. Sci. U.S.A.* **2003**, *100*, 856.

(24) Hobbs, J. D.; Shelnutt, J. A. *J. Protein Chem.* **1995**, *14*, 19.

(25) Jentzen, W.; Song, X. Z.; Shelnutt, J. A. *J. Phys. Chem. B* **1997**, *101*, 1684.

(26) Jentzen, W.; Ma, J. G.; Shelnutt, J. A. *Biophys. J.* **1998**, *74*, 753.

(27) Shelnutt, J. A. Molecular Simulations and Normal-Coordinate Structural Analysis of Porphyrins and Heme Proteins. In *Theoretical and Physical Characterization*; Kadish, K. M., Smith, K. M., Guilard, R., Eds.; The Porphyrin Handbook, Vol. 7; Academic Press: New York, 2000; p 167.

(28) Scheidt, W. R.; Lee, Y. J. *Struct. Bonding* **1987**, *64*, 1.

(29) Scheidt, W. R. Systematics of Porphyrins and Metalloporphyrins. In *Inorganic, Organometallic and Coordination Chemistry*; Kadish, K. M., Smith, K. M., Guilard, R., Eds.; The Porphyrin Handbook, Vol. 3; Academic Press: New York, 2000; p 49.

(30) Song, X.-Z.; Jentzen, W.; Jia, S.-L.; Jaquinod, L.; Nurco, D. J.; Medforth, C. J.; Smith, K. M.; Shelnutt, J. A. *J. Am. Chem. Soc.* **1996**, *118*, 12975.

(31) Medforth, C. J.; Senge, M. O.; Smith, K. M.; Sparks, L. D.; Shelnutt, J. A. *J. Am. Chem. Soc.* **1992**, *114*, 9859.

(32) Mandon, D.; Ochsenbein, P.; Fischer, J.; Weiss, R.; Jayaraj, K.; Austin, R. N.; Gold, A.; White, P. S.; Brigaud, O.; Battioni, P.; Mansuy, D. *Inorg. Chem.* **1992**, *31*, 2044.

(33) Sparks, L. D.; Medforth, C. J.; Park, M.-S.; Chamberlain, J. R.; Ondrias, M. R.; Senge, M. O.; Smith, K. M.; Shelnutt, J. A. *J. Am. Chem. Soc.* **1993**, *115*, 581.

(34) Hobbs, J. D.; Majumder, S. A.; Luo, L.; Sickelsmith, G. A.; Quirke, J. M.; Medforth, C. J.; Smith, K. M.; Shelnutt, J. A. *J. Am. Chem. Soc.* **1994**, *116*, 3261.

(35) Jentzen, W.; Simpson, M. C.; Hobbs, J. D.; Song, X.; Ema, T.; Nelson, N. Y.; Medforth, C. J.; Smith, K. M.; Veyrat, M.; Mazzanti, M.; Ramasseul, R.; Marchon, J.-C.; Takeuchi, T.; Goddard, W. A., III; Shelnutt, J. A. *J. Am. Chem. Soc.* **1995**, *117*, 5.

(36) DiMagno, S. G.; Wertsching, A. K.; Charles R. Ross, I. *J. Am. Chem. Soc.* **1995**, *117*, 8279.

(37) Parusel, A. B. J.; Wondimagegen, T.; Ghosh, A. *J. Am. Chem. Soc.* **2000**, *122*, 6371.

(38) Wertsching, A. K.; Koch, A. S.; DiMagno, S. G. *J. Am. Chem. Soc.* **2001**, *123*, 3932.

(39) Ryeng, H.; Ghosh, A. *J. Am. Chem. Soc.* **2002**, *124*, 8099.

(40) Haddad, R. E.; Gazeau, S.; Pecaut, J.; Marchon, J.-C.; Medforth, C. J.; Shelnutt, J. A. *J. Am. Chem. Soc.* **2003**, *125*, 1253.

(41) Wasbotten, I. H.; Conradie, J.; Ghosh, A. *J. Phys. Chem. B* **2003**, *107*, 3613.

(42) Brennan, T. D.; Scheidt, W. R.; Shelnutt, J. A. *J. Am. Chem. Soc.* **1988**, *110*, 3919.

(43) Alden, R. G.; Crawford, B. A.; Doolen, R.; Ondrias, M. R.; Shelnutt, J. A. *J. Am. Chem. Soc.* **1989**, *111*, 2070.

(44) Czernuszewicz, R. S.; Li, X.-Y.; Spiro, T. G. *J. Am. Chem. Soc.* **1989**, *111*, 7024.

(45) Shelnutt, J. A.; Medforth, C. J.; Berber, M. D.; Barkigia, K. M.; Smith, K. M. *J. Am. Chem. Soc.* **1991**, *113*, 4077.

(46) Piffat, C.; Melamed, D.; Spiro, T. G. *J. Phys. Chem.* **1993**, *97*, 7441.

(47) Anderson, K. K.; Hobbs, J. D.; Luo, L.; Stanley, K. D.; Quirke, J. M. E.; Shelnutt, J. A. *J. Am. Chem. Soc.* **1993**, *115*, 12346.

(48) Sparks, L. D.; Anderson, K. K.; Medforth, C. J.; Smith, K. M.; Shelnutt, J. A. *Inorg. Chem.* **1994**, *33*, 2297.

(49) Jentzen, W.; Turowska-Tyrk, I.; Schedit, W. R.; Shelnutt, H. *Inorg. Chem.* **1996**, *35*, 3559.

(50) Jentzen, W.; Unger, E.; Karvounis, G.; Shelnutt, J. A.; Dreybrodt, W.; Schweitzer-Stenner, R. *J. Phys. Chem.* **1996**, *100*, 14184.

(51) Jentzen, W.; Unger, E.; Song, X.-Z.; Jia, S.-L.; Turowska-Tyrk, I.; Schweitzer-Stenner, R.; Dreybrodt, W.; Scheidt, W. R.; Shelnutt, J. A. *J. Phys. Chem. A* **1997**, *101*, 5789.

(52) Rush, T. S.; Kozlowski, P. M.; Piffat, C. A.; Kumble, R.; Zgierski, M. Z.; Spiro, T. G. *J. Phys. Chem. B* **2000**, *104*, 5020.

(53) Ghosh, A. *Acc. Chem. Res.* **1998**, *31*, 189.

(54) Ghosh, A. Quantum Chemical Studies of Molecular Structures and Potential Energy Surfaces of Porphyrins and Hemes. In *Theoretical and Physical Characterization*; Kadish, K. M., Smith, K. M., Guilard, R., Eds.; The Porphyrin Handbook, Vol. 7; Academic Press: New York, 2000; p 1.

(55) Hoard, J. L. *Science* **1971**, *174*, 1295.

(56) Frisch, M. J.; Trucks, G. W.; Schlegel, H. B.; Scuseria, G. E.; Robb, M. A.; Cheeseman, J. R.; Zakrzewski, V. G.; Montgomery, J. A.; Stratmann, R. E.; Burant, J. C.; Dapprich, S.; Millam, J. M.; Daniels, A. D.; Kudin, K. N.; Strain, M. C.; Farkas, O.; Tomasi, J.; Barone, V.; Cossi, M.; Cammi, R.; Mennucci, B.; Pomelli, C.; Adamo, C.; Clifford, S.; Ochterski, J.; Petersson, G. A.; Ayala, P. Y.; Cui, Q.; Morokuma, K.; Malick, D. K.; Rabuck, A. D.; Raghavachari, K.; Foresman, J. B.; Cioslowski, J.; Ortiz, J. V.; Stefanov, B. B.; Liu, G.; Liashenko, A.; Piskorz, P.; Komaromi, I.; Gomperts, R.; Martin, R. L.; Fox, D. J.; Keith, T.; Al-Laham, M. A.; Peng, C. Y.; Nanayakkara, A.; Gonzalez, C.; Challacombe, M.; Gill, P. M. W.; Johnson, B. G.; Chen, W.; Wong, M. W.; Andres, J. L.; Head-Gordon, M.; Replogle, E. S.; Pople, J. A. *Gaussian 98*, revision A.9; Gaussian, Inc.: Pittsburgh, PA, 1998.

(57) Becke, A. D. *J. Chem. Phys.* **1993**, *98*, 5648

(58) Lee, C.; Yang, W.; Parr, R. G. *Phys. Rev. B* **1988**, *37*, 785.

(59) Petersson, G. A.; Al-Laham, M. A. *J. Chem. Phys.* **1991**, *94*, 6081.

(60) Tsai, H.-H. G.; Simpson, M. C. *J. Phys. Chem. A* **2003**, *107*, 526.

(61) Kozlowski, P. M.; Rush, T. S., III; Jarzecki, A. A.; Zgierski, M. Z.; Chase, B.; Piffat, C.; Ye, B.-H.; Li, X.-Y.; Peter, P.; Spiro, T. G. *J. Phys. Chem. A* **1999**, *103*, 1357.

(62) Spiro, T. G.; Czernuszewicz, R. S.; Li, X.-Y. *Coord. Chem. Rev.* **1990**, *100*, 541.

(63) Abe, M.; Kitagawa, T.; Kyogoku, Y. *J. Chem. Phys.* **1978**, *69*, 4526.

(64) Kitagawa, T.; Abe, M.; Ogoshi, H. *J. Chem. Phys.* **1978**, *69*, 4516.

(65) Vangberg, T.; Ghosh, A. *J. Am. Chem. Soc.* **1999**, *121*, 12154.

(66) Stoll, L. K.; Zgierski, M. Z.; Kozlowski, P. M. *J. Phys. Chem. A* **2003**, *107*, 4165.

(67) Stoll, L. K.; Zgierski, M. Z.; Kozlowski, P. M. *J. Phys. Chem. A* **2002**, *106*, 170.

(68) Koch, W.; Holthausen, M. C. *A Chemist's Guide to Density Functional Theory*; WILEY−VCH Verlag: Weinheim, 2000.

(69) Unger, E.; Bobinger, U.; Dreybrodt, W.; Schweitzer-Stenner, R. *J. Phys. Chem.* **1993**, *97*, 9956.

(70) Tsai, H.-H., Simpson, M. C. Manuscript in progress.

(71) Hoard, J. L. Stereochemistry of Porphyrins and Metalloporphyrins. In *Porphyrins and Metalloporphyrins*; Smith, K. M., Ed.; Elsevier: Amsterdam, 1975; p 317.

(72) Meyer, J. E. F. *Acta Crystallogr., Sect. B: Struct. Crystallogr. Cryst. Chem.* **1972**, *B28*, 2162.

(73) Cullen, D. L.; Meyer, J. E. F. *J. Am. Chem. Soc.* **1974**, *96*, 2095.

(74) Maclean, A. L.; Foran, G. J.; Kennedy, B. J.; Turner, P.; Hambley, T. W. *Aust. J. Chem.* **1996**, *49*, 1273.

(75) The experimental values for the *meso*-tetra(apopinenyl)porphyrin with the substituents arranged in aabb and abab patterns, yielding ruf = 10.8° and ruf = 26.4°, respectively, were not included in the fit because two frequencies were reported for ν_8 for these species.[35]